

Jiawen Xie¹, Pengfei Zhu¹, Jianping Hu¹, Yaguo Lyv¹ & Zhenxia Liu¹

¹ School of Power and Energy, Northwestern Polytechnical University, Xi'an 710129, China

Abstract

Void fraction is a critical parameter in the oil-air two-phase flow within the scavenge pipe of the aircraft engine lubrication system. It plays a significant role in analyzing fluid viscosity and density, pressure drop characteristics, and heat transfer performance in the scavenge pipe. Therefore, enhancing the accuracy of void fraction prediction is essential for improving the design precision of the scavenge pipe. Empirical correlations are commonly used in void fraction calculations. This study focuses on the scavenge pipe of the aircraft engine lubrication system and establishes void fraction prediction correlations based on different flow patterns to enhance prediction accuracy. High-speed photography is employed to simultaneously capture front and bottom views of the two-phase flow, constructing three-dimensional fluid images and measuring 247 void fraction data points. The extracted features from the captured images are input into machine learning methods for flow pattern identification, and the void fraction data points are classified according to different flow patterns. The performance of seven commonly used correlations is evaluated based on the classified void fraction data points. The root mean square error (RMSE) is used to determine the optimal result for each flow pattern. Results indicate that the RMSE for the void fraction correlations based on different flow patterns remains below 7.5%, significantly improving the prediction accuracy compared to using a single void fraction correlation. This improvement is of substantial importance for the design of the scavenge pipe.

Keywords: Scavenge pipe, Void fraction, Two-phase flow pattern identification, K-Nearest Neighbor Algorithm

1. Introduction

In the lubrication system of an aircraft engine, after lubricating and cooling the bearings, the oil carries a small amount of air into the scavenge pipe due to the high-speed agitation of the bearings. This results in a complex oil-air two-phase flow within the scavenge pipe. Void fraction, a fundamental parameter of two-phase flow, represents the proportion of gas within the fluid. The void fraction in the scavenge pipe directly affects the fluid's viscosity and density, which in turn influences the analysis of pressure drop and heat transfer characteristics within the pipe. Consequently, the precise calculation of the void fraction is crucial for the accurate design of the scavenge pipe.

To obtain accurate void fraction values, many scholars have conducted experimental studies and proposed various correlations. Classic correlations include those by Lockhart and Martinelli [1], Bankoff [2], Thom [3], Zivi [4], Baroczy [5], Smith [6], Beggs and Brill [7], Chisholm [8], and Gomez[9]. However, these classic correlations are limited by experimental conditions. Therefore, some researchers have developed void fraction correlations suitable for specific conditions by considering these classic correlations comprehensively. For instance, Payne [10] et al. chose three classic correlations to find a suitable void fraction correlation for two-phase flow in hilly terrain oil pipelines, finding that the Beggs and Brill correlation performed best. Parrales [11] et al. selected the most suitable correlation from 50 void fraction correlations to describe two-phase flow mechanisms in double-pipe helical vertical evaporators. Woldesemayat and Ghajar [12] compared 68 void fraction correlations and proposed a correlation considering both flow patterns and pipe inclination angle, improving the accuracy of void fraction predictions. However, these studies indicate that a single correlation is used to predict the void fraction for all flow patterns.

Void fraction in gas-liquid two-phase flow is sensitive to changes in flow patterns [13], [14]. Therefore, proposing void fraction prediction formulas for different flow patterns can significantly enhance prediction accuracy. Hasan [15] developed a void fraction prediction model for bubbly and slug flows, effectively representing void fraction data for these two flow patterns. Shi [16] et al. used experimental data to evaluate prediction errors of 12 classic void fraction correlations, demonstrating that using the same prediction model for different flow patterns is unreasonable. They subsequently established a void fraction correlation considering five flow patterns, which fit the experimental data well. Thus, establishing void fraction correlations based on different flow patterns is an effective way to improve prediction accuracy. However, most studies in this field are concentrated in the petroleum and chemical industries, with experimental media primarily being air-water. There is a lack of research on the void fraction of oil-air two-phase flow within the scavenge pipe of the aircraft engine lubrication system. Compared to the pipelines in the petroleum and chemical industries, the two-phase flow in the scavenge pipe involves actual working media and exhibits more complex properties. Therefore, it is essential to conduct research in this area.

Current measurement methods for void fraction in pipes include optical methods[17], [18], acoustic methods [19], radiation methods [20], [21], electrical methods [22], [23], [24], [25], [26], quick-closing valve methods [27], [28], and high-speed photography. These methods can be divided into invasive and non-invasive types. Invasive methods generally provide more accurate two-phase flow characteristics but can disturb the fluid flow and introduce impurities over time, causing measurement errors. Among non-invasive methods, acoustic methods are susceptible to environmental interference, radiation methods have safety issues, and tomographic imaging methods have low resolution and complex reconstruction techniques, limiting their application. High-speed photography, offering non-intrusiveness, rich information, and high sampling frequency, is widely used in experimental research and industrial applications [29], [30], [31], [32], [33], [34]. Existing high-speed photography methods typically capture fluid flow images from a single perspective and use image processing based on bubble-shape assumptions to obtain void fractions. Considering the slip and interaction between phases within the pipe, researchers have employed dual-perspective imaging to acquire more complete flow information, enabling more accurate void fraction measurements [35], [36], [37].

Reviewing the literature reveals that establishing void fraction correlations based on flow patterns can effectively enhance prediction accuracy. However, there is a lack of research on void fraction prediction correlations for different flow patterns within the scavenge pipe of the aircraft engine. This study aims to develop a void fraction prediction model for scavenge pipe based on flow patterns, using the highly reliable and widely used high-speed photography method to capture oil-air two-phase flow patterns and void fractions.

This study simulates typical operating conditions in aircraft engine scavenge pipe using high-speed photography to capture oil-air two-phase flow images from two different perspectives within the test section. Image processing techniques are employed to reconstruct the three-dimensional gas-phase image of the two-phase flow, enabling more accurate void fraction correlations. A machine learning-based flow pattern recognition model is established using the captured images. Void fractions are then classified according to the corresponding flow patterns, and void fraction correlations are developed for different flow patterns. The second part of this article details the experimental setup, the third section introduces the methods used to establish the void fraction correlation, the fourth section presents the calculation results, and the fifth section summarizes the conclusions and prospects for future research.

2. Experimental Set-up

2.1 Introduction to the Experimental System

The schematic diagram of the experimental system is shown in Figure 1. The experimental system consists of an oil supply system, an air supply system, an oil return system, and a multi-angle image acquisition system. The oil supply system and air supply system transport pure lubricating oil and air to the oil-air mixing section, respectively. The oil supply system comprises a lubricating oil tank, a solenoid valve (J4V310-08B), an oil pump (YCB1-1), a lubricating oil filter (WUA63 200P), a lubricating oil flow meter (80F08-1082/0, with an accuracy of 0.1%), and a check valve. The lubricating oil passes

through these devices in sequence before entering the mixing section. The air supply system consists of an air compressor, an air tank, a solenoid valve, a dryer, an air filter, an air flowmeter (JFQ20D107745, with an accuracy of 1% F.S), and a check valve. After the lubricating oil and air mixture thoroughly in the mixer, they enter the experimental pipeline. The multi-angle image acquisition system includes the experimental pipeline, an isosceles prism, panel light sources, a high-speed camera (X213), and data acquisition equipment. After collecting fluid information through the multi-angle image acquisition system, the oil-air mixture enters the oil return system. The oil return system separates the oil-air mixture in the experimental pipeline. The oil-air mixture is pumped into the oil-air separator (YCB2.5/0.6-2), where the air is discharged into the atmosphere, and the remaining lubricating oil is cooled by a heat exchanger (AH1012-3P-CA3/B) before being recycled in the lubricating oil tank.

As shown in Figure 1, in the arrangement of the multi-angle image acquisition system, one right-angle side of the isosceles prism is close to the experimental pipeline, and the other right-angle side is perpendicular to the imaging plane of the high-speed camera. The 45° reflective surface reflects the bottom flow image of the pipeline, enabling the high-speed camera to simultaneously capture both the front and the reflected bottom flow images of the pipeline.

The inner diameter of the experimental pipeline is 14 mm. The experiment is conducted at room temperature, with 4050 lubricating oil and air as the experimental media, having densities of 972.2 kg/m³ and 1.205 kg/m³, respectively, under normal temperature. The experimental range is as follows: air flow rate ranging from 0.1 to 31.623 m/s and lubricating oil flow rate ranging from 0.25 to 1 m/s.

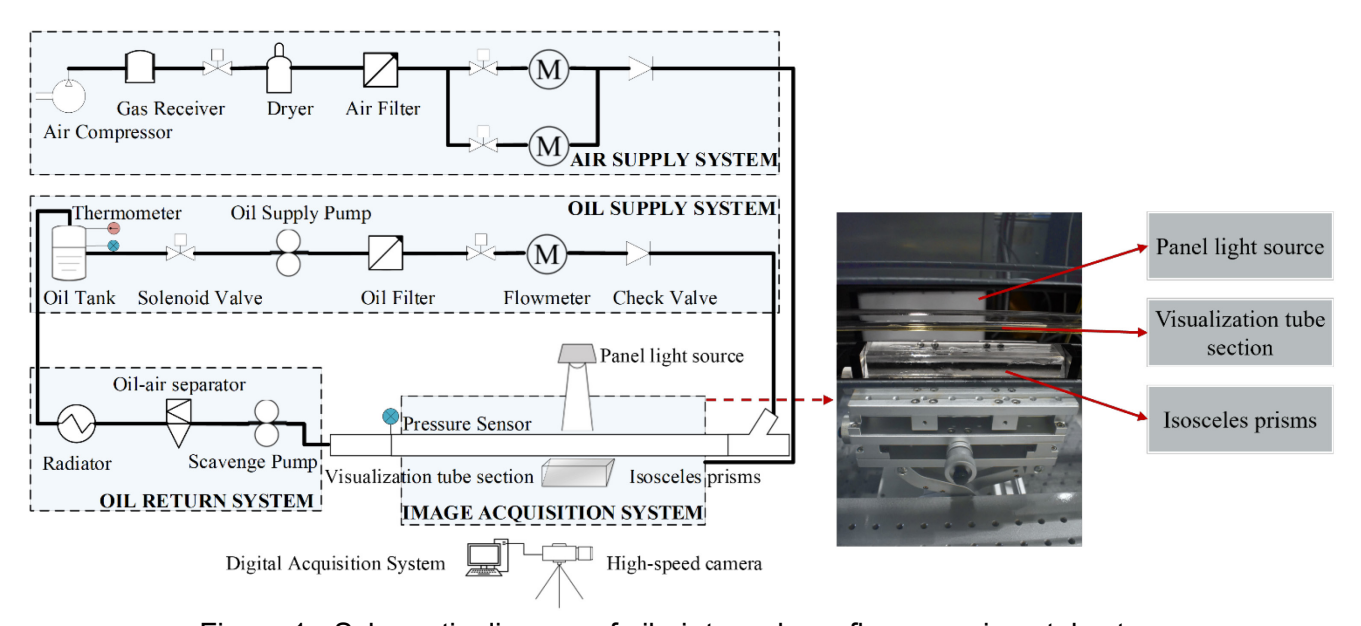


Figure 1 - Schematic diagram of oil-air two-phase flow experimental setup

2.2 Datasets

Before establishing void fraction correlations for different flow patterns in the scavenge pipe under various experimental conditions, it is necessary to identify the flow patterns in the fluid flow images from the experiment. The purpose of identifying flow patterns is to classify the images, which facilitates the establishment of different void fraction correlations. The flow pattern recognition model is built using the machine learning method, with the input data for machine learning referred to as the dataset. The choice of dataset affects the results of flow pattern recognition. Therefore, the dataset used for the recognition model is introduced next.

In the experiment described in section 2.1, four different flow patterns were obtained: plug flow, stratified flow, wavy flow, and annular flow. Figure 2 presents typical images of these four flow patterns. The recognition model's dataset will be derived from these images.

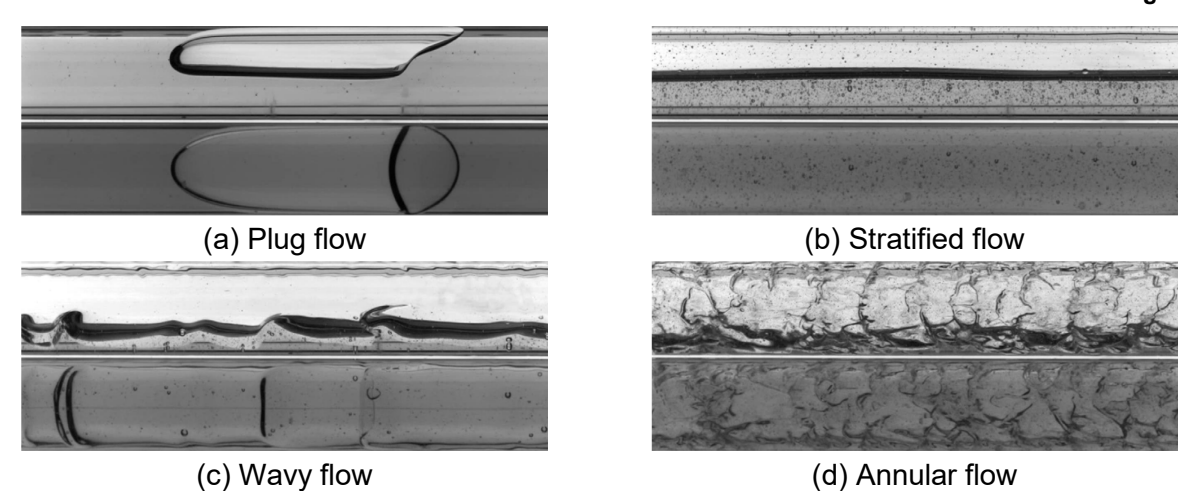


Figure 2 - Schematic diagram of oil-air two-phase flow experimental setup

To distinguish different flow patterns, features that can differentiate between the flow pattern categories need to be extracted from the images. Wavelet packet decomposition is a feature extraction method. After performing digital image preprocessing on the experimental flow pattern images, wavelet packet decomposition is used to extract features from the dataset images, yielding seven features: first-layer wavelet decomposition energy, second-layer wavelet decomposition energy, first-layer wavelet decomposition norm, second-layer wavelet decomposition norm, mean, approximate coefficient variance, and information entropy. The dataset for the recognition model consists of these extracted features.

It is important to note that differences in the number of samples for each category in the dataset can complicate the training process of the recognition model. To prevent issues arising from class imbalance, 1000 sample images for each flow pattern were included in the dataset, totaling 4000 images. The dataset is divided into the training and testing set, used for training the recognition model and evaluating its recognition capability, respectively. The number of samples in the training and testing set follows a 4:1 ratio. The distribution of samples in the dataset is shown in Table 1.

Table 1 Sample distribution for flow pattern recognition model

Flow pattern	Plug flow	Stratified flow	Wavy flow	Annular flow	Sum
Training data	800	800	800	800	3200
Testing data	200	200	200	200	800

3. Methods

3.1 Flow Pattern Recognition Model

It is essential to establish a highly accurate flow pattern recognition model to improve the accuracy of void fraction prediction models based on different flow patterns. This study selects the K-nearest neighbor (KNN) method as the flow pattern recognition model. The following is an introduction to the KNN method.

The KNN algorithm is a simple and easily understandable algorithm that can overcome the problem of linear inseparability and is suitable for multi-classification problems. Figure 3 shows the schematic diagram of the KNN algorithm, where the horizontal and vertical coordinates represent two different features extracted from the sample. The dots in the figure represent sample objects, with different colors indicating different categories. The gray dot is the new sample point to be predicted. The KNN algorithm predicts the category of the new sample point based on the K nearest points. When K=3, as shown by the black dashed circle, the green category 1 sample points outnumber the yellow

category 2 sample points, so the prediction is category 1. When K=5, as shown by the black solid circle, the yellow category 2 sample points outnumber the green category 1 sample points, so the prediction is category 2. Therefore, the choice of K value is crucial in the KNN algorithm.

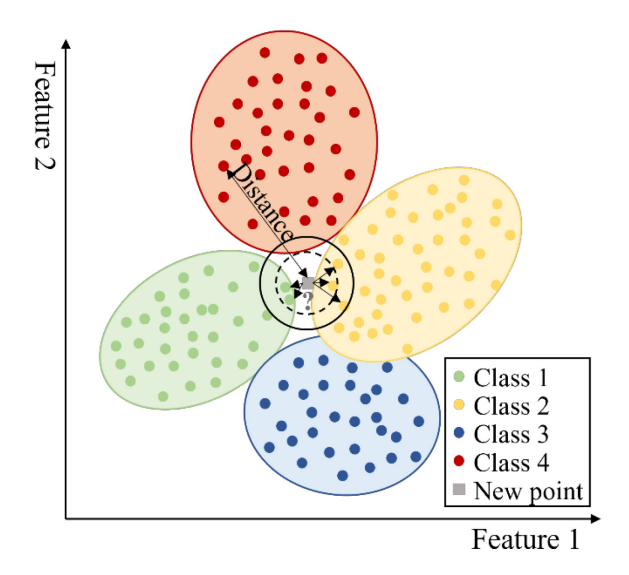


Figure 3 - Schematic diagram of the K-nearest neighbor algorithm

After inputting the training dataset from Section 2.2 into the KNN model, the model was trained with K values ranging from 1 to 30. It was found that the training set achieved the best identification performance when K=7. Subsequently, the model's identification performance was further tested using the test set with K=7. The confusion matrix of the recognition results for the test set, input into the trained model, is shown in Figure 4. In Figure 4, '1' represents plug flow, '2' represents stratified flow, '3' represents wavy flow, and '4' represents annular flow. The recognition error of the model is small, primarily occurring between stratified flow and wavy flow due to their similarity, as seen in the images in Figure 2. Overall, the recognition accuracy for the test set is 96.63%, indicating that the recognition model can effectively distinguish the four different flow patterns.

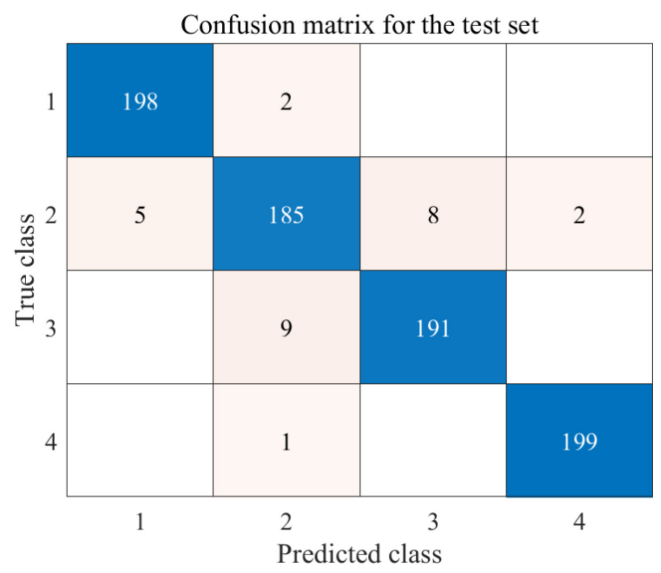


Figure 4 - Confusion matrix of flow pattern recognition model

3.2 Void Fraction Calculation Method

Calculating void fractions through digital image processing is a common method for obtaining void fractions, as shown in studies by Sukamta [29] and Huang [38], among others. These studies derive void fractions by counting the gas phase pixel numbers in single-view binary flow pattern images. However, this method only considers the two-dimensional characteristics of two-phase flow along

the axial section of a circular pipe. For the specific structure of cylindrical pipes, the transverse section also contains information on the gas phase distribution. Therefore, extracting information from a single view can lead to inaccuracies in void fraction calculations.

By capturing flow images from a vertical view of the pipeline, it is possible to reconstruct a threedimensional image of the fluid and calculate the volumetric void fraction. The volumetric void fraction comprehensively reflects the gas phase proportion in the two-phase flow, and the three-dimensional image of the fluid provides information on the gas phase distribution. This method will be used to obtain a more accurate void fraction in this section.

Figure 5 shows the original image and the binary image obtained through digital image processing. By scanning the gas phase pixel information in the binary image, the obtained pixel information serves as input for reconstructing the three-dimensional image. Assuming that the bubble surface is smooth and the cross-section in the radial direction is elliptical, the binary images from the two views provide the major and minor axis information of the ellipse. By scanning the number of white pixels in the binary image, the major and minor axis information is obtained. After drawing the elliptical cross-section of each bubble in the radial direction, the ellipses are stacked along the axial direction to complete the three-dimensional reconstruction of the bubble.



Figure 5 - Original and binary image obtained through digital image processing

As previously discussed, the KNN algorithm achieves a flow pattern recognition accuracy of 96.63%, effectively distinguishing different flow patterns. Therefore, the predicted image features are input into the recognition model to obtain the corresponding category, and the void fraction is calculated using the following formulas:

$$V_{pipe} = \sum_{i=1}^{N} \frac{1}{4} \times \pi \times (\lambda \times d)^{2} \times \lambda$$
 (1)

$$V_{g s lug} = \sum_{k=1}^{n} \sum_{i=1}^{l_k} \frac{1}{4} \times \pi \times (\lambda \times d_{(k,i)})^2 \times \lambda$$
 (2)

$$\phi_{slug} = \frac{V_{gslug}}{V_{pipe}} = \frac{\sum_{k=1}^{n} \sum_{i=1}^{l_k} d_{(k,i)}^2}{N \times d^2}$$
(3)

$$V_{gwavy} = \sum_{i=1}^{N} \left[\frac{\pi}{4} \times d^{2} + \sqrt{h_{i} \times d - h_{i}^{2}} \times (h_{i} - \frac{d}{2}) - \frac{d^{2}}{4} \times ar \cos(2 \times \frac{h_{i}}{d} - 1) \right] \times \lambda^{3}$$
 (4)

$$\phi_{wavy} = \phi_{stratified} = \frac{V_{gwavy}}{V_{nine}} = \frac{1}{N} \sum_{i=1}^{N} \left[1 + \frac{4}{\pi d^2} \sqrt{h_i \times d - h_i^2} \times (h_i - \frac{d}{2}) - \frac{1}{\pi} \times arc \cos(2 \times \frac{h_i}{d} - 1) \right]$$
 (5)

$$V_{gannular} = \sum_{i=1}^{N} \frac{1}{4} \times \pi \times (\lambda \times d_i)^2 \times \lambda$$
 (6)

$$\phi_{annular} = \frac{V_{gannular}}{V_{pipe}} = \frac{\sum_{i=1}^{N} d_i^2}{N \times d^2}$$
(7)

The parameter n refers to the n-th gas bubble in the plug flow. The parameter l_k denotes the length of the k-th gas slug. The parameter $d_{(k,i)}$ represents the number of pixels in the cross-sectional height at pixel i. The parameter d refers to the diameter of the pipe. The parameter λ represents the actual length per pixel. The parameter N denotes the number of pixels in the image width.

While calculating the void fraction, the three-dimensional image is constructed simultaneously. The three-dimensional images of four typical flow patterns are shown in Figure 6:

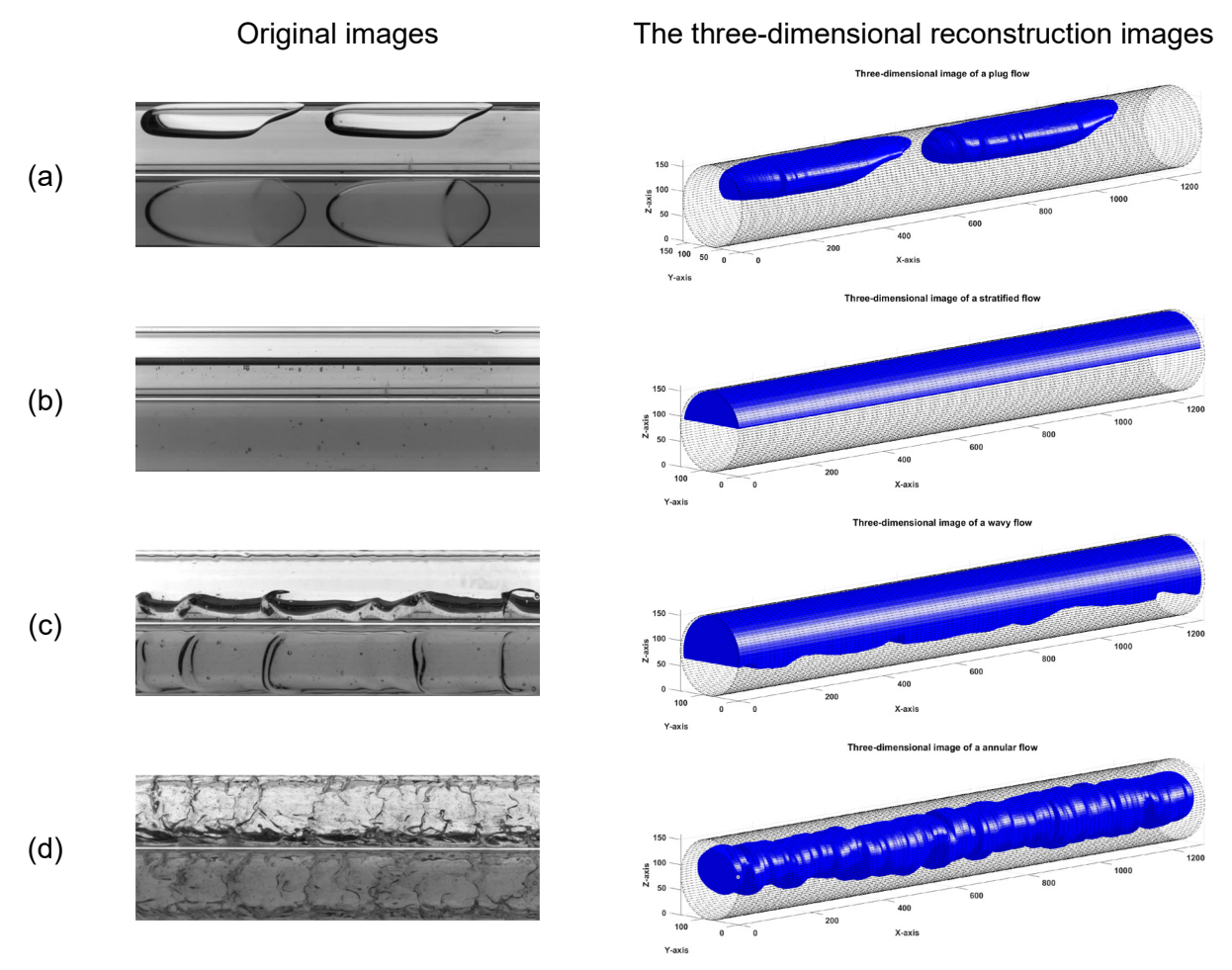


Figure 6 - Three-dimensional reconstruction images of flow patterns: (a) plug flow; (b) stratified flow; (c) wavy flow; (d) annular flow

These three-dimensional images better reflect the spatial distribution and flow characteristics of the flow patterns, significantly improving the accuracy of void fraction and gas phase spatial distribution measurements. In void fraction calculation, the binary image from digital image processing provides the axial section void fraction, and the transverse section void fraction can be obtained from the sliced images. Additionally, combining three-dimensional and transverse section images allows for the calculation of volumetric void fraction, enhancing measurement accuracy.

3.3 Void Fraction Calculation Correlation

On the one hand, the void fraction can be obtained through the void fraction calculation method described in section 3.2. On the other hand, existing void fraction correlations from the literature are

used to calculate the void fraction under different experimental conditions, resulting in a predicted void fraction. By comparing the experimentally measured void fraction with the void fraction predicted by the correlations for different flow patterns, the suitable void fraction correlations for different flow patterns can be identified.

Seven existing void fraction correlations were selected from the literature, as shown in Table 2. These correlations were used to calculate the void fraction for different flow patterns, and the calculated values were compared with the measured void fraction values for each flow pattern. The experimental conditions for different flow patterns are listed in Table 3.

Table 2 Correlations for void fraction.

Author	Void fraction correlation		
Lockhart-Martinelli (1949)	$\alpha_{v} = [1 + 0.28((1-x)/x)^{0.64}(\rho_{l}/\rho_{g})^{0.36}(\rho_{l}/\rho_{g}))^{0.07}]^{-1}$		
Flanigan (1958)	$\alpha_{v} = \left[1 + 3.063(J_g)^{-1.006}\right]^{-1}$		
Baroczy (1966)	$\alpha_v = [1 + ((1-x)/x)^{0.74} (\rho_l/\rho_g)^{0.65} (\rho_l/\rho_g))^{0.13}]^{-1}$		
Mattar and Gregory (1974)	$\alpha_{v} = J_{g} \left[1.3(J_{g} + J_{l}) + 0.7 \right]^{-1}$		
Mishima and Hibiki (1996)	$\alpha_v = J_g \left[(1.2 + 0.51 \exp(-0.691D))(J_g + J_l) \right]^{-1}$		
Jowitt (1982)	$\alpha_{v} = J_{g} \left\{ [1 + 0.796 exp(-0.061(\rho_{l} / \rho_{g}))](J_{g} + J_{l}) + 0.034((\rho_{l} / \rho_{g}) - 1.000) \right\}$		
Bestion (2002)	$\alpha_v = J_g \left[(J_g + J_l) + 0.188(gD \rho_l - \rho_g \rho_g)^{0.25} \right]^{-1}$		

Table 4 Number of data points for different flow patterns

Flow patterns	Number of points		
Plug flow	79		
Stratified flow	58		
Wavy flow	60		
Annular flow	50		

4. Result

To evaluate the predictive capability of the void fraction correlations in section 3.3, the root mean square error (RMSE) was used. Equation 8 provides the expression for RMSE.

$$RMSE = \left\{ 1/(n-1) \sum_{i=1}^{n} \left[\alpha_{v,predicted}(i) - \alpha_{v,measured}(i) \right]^{2} \right\}^{0.5}$$
(8)

After comparing the void fraction correlations with the experimental values, the RMSE for each correlation in each flow pattern was obtained, as shown in Table 5. Among the seven void fraction correlations, the prediction accuracy varies for different flow patterns. The best-performing void fraction correlation also varies among the different flow patterns. The Bestion correlation performs

best for plug flow, the Lockhart-Martinelli correlation for stratified flow, the Mishima and Hibiki correlation for wavy flow, and the Mattar and Gregory correlation for annular flow. The RMSE between the predicted and measured void fractions is less than 7.5% for these correlations. Therefore, establishing void fraction correlations based on different flow patterns can improve prediction accuracy.

Table 5 - RMSE of void fraction prediction for different flow patterns using different correlations

Author	Plug flow	Stratified flow	Wavy flow	Annular flow
Lockhart and Martinelli	6.44%	7.48%	24.14%	9.21%
Flanigan	10.74%	24.08%	9.75%	7.37%
Baroczy	9.82%	16.5%	17.43%	9.27%%
Mattar and Gregory	7.42%	9.48%	14.04%	4.77%
Mishima and Hibiki	8.01%	10.95%	7.13%	14.25%
Jowitt	7.61%	10.68%	19.1%	6.33%
Bestion	5.67%	14.16%	33.57%	7.3%

Figure 7 to Figure 10 show the predictive performance of the best void fraction correlations for the four flow patterns. It can be observed that the prediction deviation of the void fraction correlations in Figure 7 to Figure 10 mostly remains within ±10%.

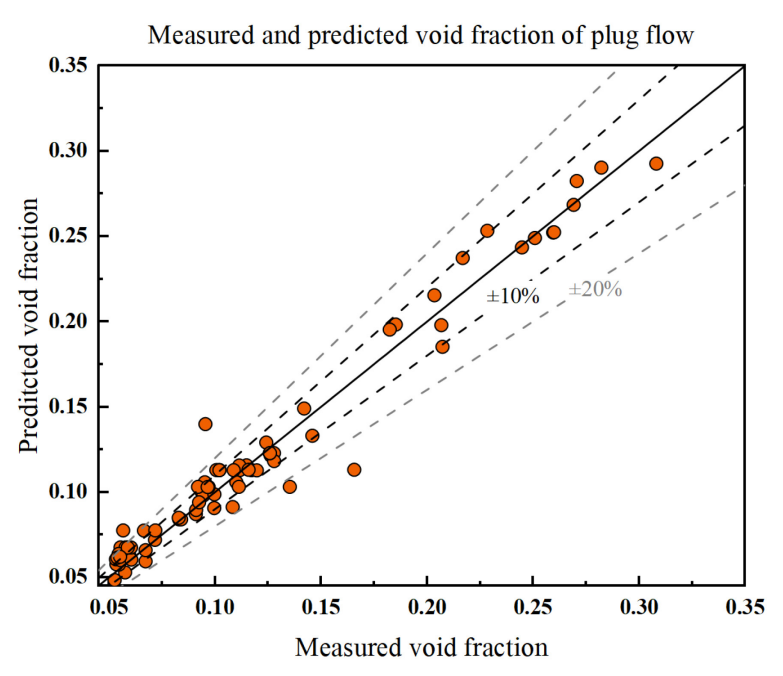


Figure 7 – Predictive performance of the Bestion correlation for void fraction in plug flow

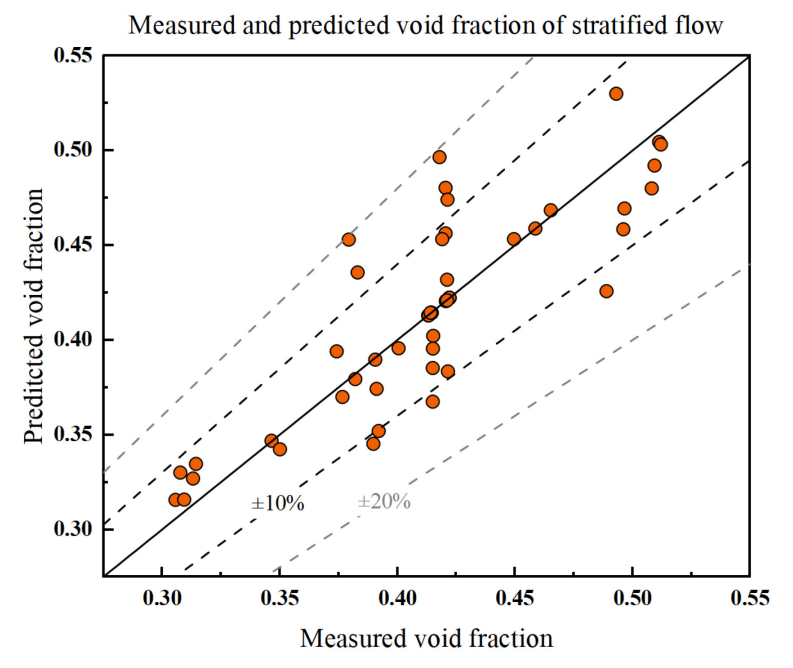


Figure 8 – Predictive performance of the Lockhart-Martinelli correlation for void fraction in stratified flow

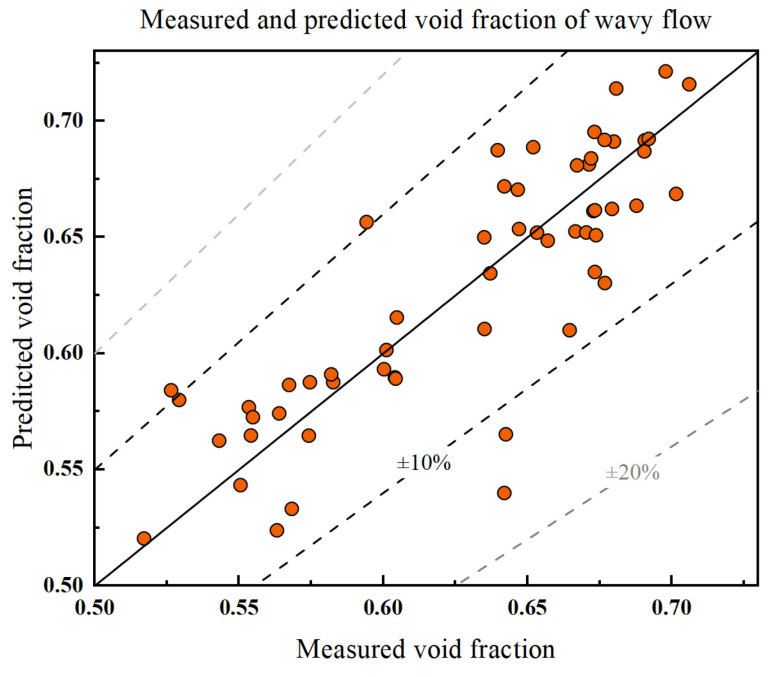


Figure 9 – Predictive performance of the Mishima and Hibiki correlation for void fraction in wavy flow

Measured and predicted void fraction of annular flow

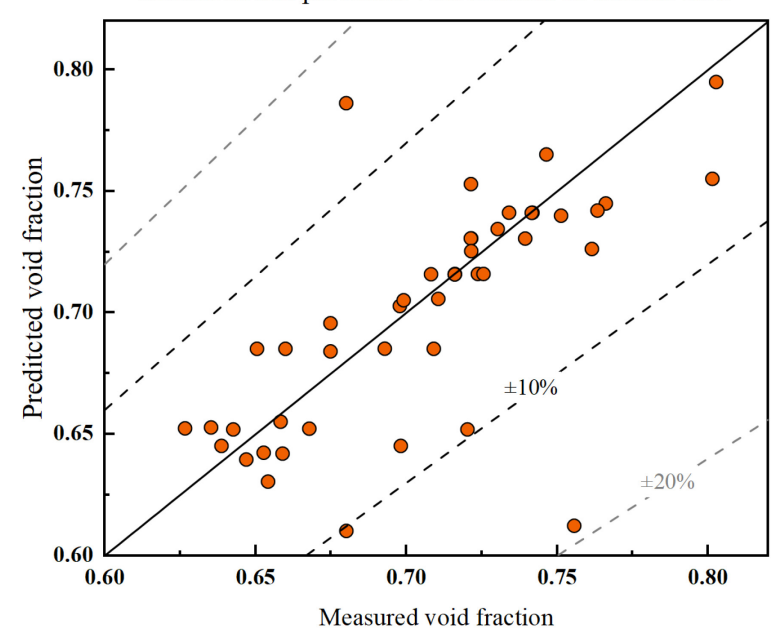


Figure 10 – Predictive performance of the Mattar and Gregory correlation for void fraction in annular flow

5. Conclusion

This study investigates the void fraction of oil-air two-phase flow in the scavenge pipe of an aeroengine lubrication system. To enhance the accuracy of void fraction prediction, void fraction
correlations based on different flow patterns were established. First, the KNN flow pattern recognition
model was developed using frontal and bottom views of oil-air two-phase flow captured by highspeed photography. This recognition model achieved a flow pattern identification rate of 96.63%.
The model was then used to classify the flow images under various conditions. Next, a threedimensional model of the two-phase flow was constructed to calculate the void fraction for different
experimental conditions. Finally, the predictive capabilities of seven existing void fraction correlations
were evaluated, and the four best correlations were selected for predicting the void fraction in the
scavenge pipe's oil-air two-phase flow. The main conclusions are as follows:

- 1. Among the seven existing void fraction correlations, none can accurately predict the void fraction for all flow patterns, consistent with the findings of Shi et al. [16]. Therefore, selecting the best void fraction correlation for each flow pattern can effectively improve the accuracy of void fraction prediction in the scavenge pipe's oil-air two-phase flow.
- 2. Through evaluation and analysis of the existing correlations, the best-performing void fraction correlation for each flow pattern was identified, with the RMSE kept below 7.5%, and most data points having a prediction error within ±10%. Therefore, it can be considered that under conditions similar to those in this study, the Bestion correlation can be selected to predict the void fraction for Plug flow, the Lockhart-Martinelli correlation for Stratified flow, the Mishima and Hibiki correlation for Wavy flow, and the Mattar and Gregory correlation for Annular flow. This selection can ensure prediction accuracy to a certain extent.

Since a supervised classification model, such as the K-nearest neighbor method, introduces some subjectivity, future research will aim to reduce this subjectivity and increase the dataset size to establish a more broadly applicable void fraction prediction model.

6. Acknowledgments

This work was supported by the National Science and Technology Major Project (J2019-III-0023-0067) In China.

7. Contact Author Email Address

The contact author phone number: 18392017729. The email address: zhupengfei@nwpu.edu.cn.

8. Copyright Statement

The authors confirm that they, and/or their company or organization, hold copyright on all of the original material included in this paper. The authors also confirm that they have obtained permission, from the copyright holder of any third party material included in this paper, to publish it as part of their paper. The authors confirm that they give permission, or have obtained permission from the copyright holder of this paper, for the publication and distribution of this paper as part of the ICAS proceedings or as individual off-prints from the proceedings.

References

- [1] W Lockhart R, "Proposed Correlation of Data for Isothermal Two-Phase, Two-Component Flow in Pipes," *Chem Eng Progr*, vol. 45, pp. 39–48, 1949.
- [2] Bankoff S G. "A Variable Density Single-Fluid Model for Two-Phase Flow With Particular Reference to Steam-Water Flow," *J. Heat Transf.*, vol. 82, no. 4, pp. 265–272, Nov. 1960, doi: 10.1115/1.3679930.
- [3] Thom J R S. "Prediction of pressure drop during forced circulation boiling of water," *Int. J. Heat Mass Transf.*, vol. 7, no. 7, pp. 709–724, Jul. 1964, doi: 10.1016/0017-9310(64)90002-X.
- [4] Zivi S M. "Estimation of Steady-State Steam Void-Fraction by Means of the Principle of Minimum Entropy Production," *J. Heat Transf.*, vol. 86, no. 2, pp. 247–251, May 1964, doi: 10.1115/1.3687113.
- [5] Baroczy C J. "SYSTEMATIC CORRELATION FOR TWO-PHASE PRESSURE DROP.," *Chem Eng Progr Symp Ser 62 No 64 232-491966*, Jan. 1966, Accessed: Apr. 24, 2024. [Online]. Available: https://www.osti.gov/biblio/4300603
- [6] Smith S L. "Void Fractions in Two-Phase Flow: A Correlation Based upon an Equal Velocity Head Model," *Proc. Inst. Mech. Eng.*, vol. 184, no. 1, pp. 647–664, Jun. 1969, doi: 10.1243/pime_proc_1969_184_051_02.
- [7] Beggs D H and Brill J P. "A Study of Two-Phase Flow in Inclined Pipes," J. Pet. Technol., vol. 25, no. 05, pp. 607–617, May 1973, doi: 10.2118/4007-PA.
- [8] Chisholm D. "Pressure gradients due to friction during the flow of evaporating two-phase mixtures in smooth tubes and channels," *Int. J. Heat Mass Transf.*, vol. 16, no. 2, pp. 347–358, Feb. 1973, doi: 10.1016/0017-9310(73)90063-X.
- [9] Gomez L E, Shoham O, and Taitel Y, "Prediction of slug liquid holdup: horizontal to upward vertical flow," *Int. J. Multiph. Flow*, vol. 26, no. 3, pp. 517–521, Mar. 2000, doi: 10.1016/S0301-9322(99)00025-7.
- [10] Payne G A, Palmer C M, Brill J P, and Beggs H D. "Evaluation of Inclined-Pipe, Two-Phase Liquid Holdup and Pressure-Loss Correlation Using Experimental Data (includes associated paper 8782)," *J. Pet. Technol.*, vol. 31, no. 09, pp. 1198–1208, Sep. 1979, doi: 10.2118/6874-PA.
- [11] Parrales A, Colorado D, Huicochea A, Díaz J, and Alfredo Hernández J. "Void fraction correlations analysis and their influence on heat transfer of helical double-pipe vertical evaporator," *Appl. Energy*, vol. 127, pp. 156–165, Aug. 2014, doi: 10.1016/j.apenergy.2014.04.036.
- [12] Woldesemayat M. A and Ghajar A J. "Comparison of void fraction correlations for different flow patterns in horizontal and upward inclined pipes," *Int. J. Multiph. Flow*, vol. 33, no. 4, pp. 347–370, Apr. 2007, doi: 10.1016/j.ijmultiphaseflow.2006.09.004.
- [13] Zhao Y, Bi Q, and Hu R. "Recognition and measurement in the flow pattern and void fraction of gas-liquid two-phase flow in vertical upward pipes using the gamma densitometer," *Appl. Therm. Eng.*, vol. 60, no. 1–2, pp. 398–410, Oct. 2013, doi: 10.1016/j.applthermaleng.2013.07.006.
- [14] Cheng L. Frontiers and Progress in Multiphase Flow I. Cham: Springer International Publishing, 2014. doi: 10.1007/978-3-319-04358-6.
- [15] Hasan A R. "Void Fraction in Bubbly and Slug Flow in Downward Vertical and Inclined Systems," *SPE Prod. Facil.*, vol. 10, no. 03, pp. 172–176, Aug. 1995, doi: 10.2118/26522-PA.
- [16] Shi S, Wang Y, Qi Z, Yan W, and Zhou F. "Experimental investigation and new void-fraction calculation method for gas—liquid two-phase flows in vertical downward pipe," *Exp. Therm. Fluid Sci.*, vol. 121, p. 110252, Feb. 2021, doi: 10.1016/j.expthermflusci.2020.110252.
- [17] Kong W, Li S, Hao H, Yan P, Zhuo C, and Li H. "Measurement method of gas holdup in horizontal gas-liquid two-phase flow based on fiber-optic probe array," *Flow Meas. Instrum.*, vol. 97, p. 102588, Jul. 2024, doi: 10.1016/j.flowmeasinst.2024.102588.
- [18] Hao H, Hao B, Kong W, Chen J, and Zhang X. "Phase volume fraction measurement of vertical oil—water-gas flow using integrated optical-electrical coaxial cross-modal probe sensor," *Exp. Therm. Fluid Sci.*, vol. 150, p. 111045, Jan. 2024, doi: 10.1016/j.expthermflusci.2023.111045.
- [19] Ren W, Jin N, and Zhang J. "Modelling of ultrasonic method for measuring gas holdup of Oil-Gas-Water three phase flows," *Ultrasonics*, vol. 124, p. 106740, Aug. 2022, doi: 10.1016/j.ultras.2022.106740.
- [20] M Roshani *et al.* "Evaluation of flow pattern recognition and void fraction measurement in two phase flow independent of oil pipeline's scale layer thickness," *Alex. Eng. J.*, vol. 60, no. 1, pp. 1955–1966, Feb. 2021, doi: 10.1016/j.aej.2020.11.043.
- [21] Wei Z *et al.* "Void Fraction Measurement Using the Coaxial Line Phase Sensor in the Vertical Gas-Liquid Slug Flow," *IEEE Sens. J.*, vol. 22, no. 2, pp. 1346–1355, Jan. 2022, doi: 10.1109/JSEN.2021.3130722.
- [22] Kim S, Fu X Y, Wang X, and Ishii M. "Development of the miniaturized four-sensor conductivity probe and the signal processing scheme," *Int. J. Heat Mass Transf.*, vol. 43, no. 22, pp. 4101–4118, Nov. 2000, doi: 10.1016/S0017-9310(00)00046-6.
- [23] Qu X, Guo Q, Zhang Y, Qi X, and Liu L. "A New Vector-Based Signal Processing Method of Four-Sensor Probe for Measuring Local Gas-Liquid Two-Phase Flow Parameters Together with Its Assessment against One Bubbly Flow," *Appl. Sci.*, vol. 10, no. 16, Art. no. 16, Jan. 2020, doi: 10.3390/app10165463.
- [24] He D, Chen S, and Bai B. "Void fraction measurement of stratified gas-liquid flow based on multi-wire capacitance probe," *Exp. Therm. Fluid Sci.*, vol. 102, pp. 61–73, Apr. 2019, doi: 10.1016/j.expthermflusci.2018.11.005.
- [25] Bowden R C, Lessard É, and Yang S-K. "Void fraction measurements of bubbly flow in a horizontal 90° bend using wire mesh sensors," *Int. J. Multiph. Flow*, vol. 99, pp. 30–47, Feb. 2018, doi: 10.1016/j.ijmultiphaseflow.2017.09.009.

- [26] Huang Z, Wang B, and Li H. "Application of electrical capacitance tomography to the void fraction measurement of two-phase flow," *IEEE Trans. Instrum. Meas.*, vol. 52, no. 1, pp. 7–12, Feb. 2003, doi: 10.1109/TIM.2003.809087.
- [27] Qian H and Hrnjak P. "Void fraction measurement and flow regimes visualization of R134a in horizontal and vertical ID 7 mm circular tubes," *Int. J. Refrig.*, vol. 103, pp. 191–203, Jul. 2019, doi: 10.1016/j.ijrefrig.2019.04.018.
- [28] "Measurement of the void fraction of R-134a flowing through a horizontal tube," *Int. Commun. Heat Mass Transf.*, vol. 56, pp. 8–14, Aug. 2014, doi: 10.1016/j.icheatmasstransfer.2014.04.004.
- [29] Sukamta S and Sudarja S. "Correlation between Void Fraction and Two-Phase Flow Pattern Air-Water with Low Viscosity in Mini Channel with Slope 30 Degrees," *Key Eng. Mater.*, vol. 846, pp. 289–295, 2020, doi: 10.4028/www.scientific.net/KEM.846.289.
- [30] Płaczkowski K S "Application of photographic technology to the two-phase flow regime recording and concurrent void fraction quantification," thesis, Institute of Mechanical Engineering, 2020. Accessed: Apr. 24, 2024. [Online]. Available: https://repo.pw.edu.pl/info/phd/WUT98b8085e646d40d6a8c3bf7439da6997/?ps=20&lang=en&pn=1
- [31] Han J, Liu Y, Chu W, Zhao C, and Bo H. "Experimental study on visualized flow boiling in a narrow rectangular channel," *Int. Commun. Heat Mass Transf.*, vol. 138, p. 106383, Nov. 2022, doi: 10.1016/j.icheatmasstransfer.2022.106383.
- [32] Serra P L S, Masotti P H F, Rocha M S, Andrade D A de, Torres W M, and Mesquita R N de, "Two-phase flow void fraction estimation based on bubble image segmentation using Randomized Hough Transform with Neural Network (RHTN)," *Prog. Nucl. Energy*, vol. 118, p. 103133, Jan. 2020, doi: 10.1016/j.pnucene.2019.103133.
- [33] Bowers C, "Determination of Void Fraction in Separated Two-Phase Flows Using Optical Techniques," Jan. 2010, Accessed: Apr. 24, 2024. [Online]. Available: https://www.academia.edu/9098706/Determination_of_Void_Fraction_in_Separated_Two_Phase_Flows_Using_Optical_Techniques
- [34] Singh S G, Jain A, Sridharan A, Duttagupta S P, and Agrawal A. "Flow map and measurement of void fraction and heat transfer coefficient using an image analysis technique for flow boiling of water in a silicon microchannel," *J. Micromechanics Microengineering*, vol. 19, no. 7, p. 075004, Jun. 2009, doi: 10.1088/0960-1317/19/7/075004.
- [35] Zhang J, Sunden B, Wadekar V, and Wu Z. "3D gas-liquid interfaces and flow characteristics of two-phase flows in horizontal tubes," *J. Phys. Conf. Ser.*, vol. 2116, no. 1, p. 012072, Nov. 2021, doi: 10.1088/1742-6596/2116/1/012072.
- [36] Zhang J, Huang N, Lei L, Liang F, Wang X, and Wu Z. "Studies of gas-liquid two-phase flows in horizontal mini tubes using 3D reconstruction and numerical methods," *Int. J. Multiph. Flow*, vol. 133, p. 103456, Dec. 2020, doi: 10.1016/j.ijmultiphaseflow.2020.103456.
- [37] Fu X, Zhang P, Hu H, Huang C J, Huang Y, and Wang R Z, "3D visualization of two-phase flow in the micro-tube by a simple but effective method," *J. Micromechanics Microengineering*, vol. 19, no. 8, p. 085005, Aug. 2009, doi: 10.1088/0960-1317/19/8/085005.
- [38] Huang L, Wen S, Liu Y, Lin Z, and He Z, "Development of a fluorescence imaging method to measure void fractions of gas-liquid two-phase flows in a small tube-window for transparent fluids," *Meas. Sci. Technol.*, vol. 31, no. 4, p. 045301, Apr. 2020, doi: 10.1088/1361-6501/ab4dee.